

Source apportionment and formation of warm season ozone pollution in Chengdu based on CMAQ-ISAM

Yaohan Xian^a, Yang Zhang^{a,b,*}, Zhihong Liu^{a,b}, Haofan Wang^c, Junjie Wang^a, Chao Tang^a

^a College of Resources and Environment, Chengdu University of Information Technology, Chengdu 610225, China

^b Chengdu Plain Urban Meteorology and Environment Observation and Research Station of Sichuan Province, Chengdu University of Information Technology, Chengdu 610225, China

^c School of Atmospheric Sciences, Sun Yat-sen University, and Southern Marine Science and Engineering Guangdong Laboratory (Zhuhai), Zhuhai 519082, China

ARTICLE INFO

Keywords:

Ozone
Air quality model
Source apportionment
Chengdu

ABSTRACT

In this study, the WRF-CMAQ model integrated with BEM urban canopy model was used to simulate the concentrations of Ozone (O_3) and its precursors, NO_x and VOCs, in warm season of Chengdu, conduct source apportionment and formation analysis. The results show that the O_3 in Chengdu exhibits a west-high/east-low spatial pattern, attributable to nearly 40% contribution from boundary sources representing the transport role of the Sichuan Basin, regional sources from districts emitting high precursor concentrations, and increasing biogenic contributions from western areas due to rising BVOCs emissions during the warm season. NO_x from traffic and VOCs from industrial sources, both prevalent in Chengdu's high urban density areas, chemically react to form O_3 , making these sectors primary contributors to O_3 . NO_x photochemical reactions producing O_3 occur at 150 m–2500 m with peak generation rates of $10 \mu\text{g}/(\text{m}^3 \cdot \text{hr})$. Ground-level NO titration removal is most significant during heavy traffic (14:00–21:00), ranging from -70 to $-200 \mu\text{g}/(\text{m}^3 \cdot \text{hr})$. O_3 is replenished through similar rates of daytime vertical diffusion and nighttime horizontal advection, correlating with urban density across regions. Controlling Chengdu's warm season O_3 requires focusing on long-distance external transport and regional precursor emission reductions, with strategies tailored to local urban characteristics.

1. Introduction

Tropospheric ozone (O_3) is an important component of the atmosphere and is crucial in atmospheric chemistry. Tropospheric O_3 is also a secondary pollutant formed by a series of photochemical reactions between nitrogen oxides (NO_x) and volatile organic compounds (VOCs) under solar radiation (Li et al., 2019), with many adverse effects on human health, global ecosystems, and climate (Arneth et al., 2010; Cohen et al., 2017). In recent years, with China's rapid industrial and economic development and the expansion of urban areas, high concentrations of O_3 pollution have frequently occurred in densely populated urban areas such as the Beijing-Tianjin-Hebei region, the Pearl River Delta, the Yangtze River Delta, and the Sichuan Basin (Liu et al., 2020; Yu et al., 2019). Therefore, preventing and controlling O_3 pollution have become popular topics in China's atmospheric environment.

* Corresponding author at: College of Resources and Environment, Chengdu University of Information Technology, Chengdu 610225, China
E-mail address: zhangyang@cuit.edu.cn (Y. Zhang).

To study the prevention and control of O₃ pollution, it is crucial to understand its precursors, NO_x (NO, NO₂), and VOCs. Under light conditions, NO₂ generates NO and O₃. In the absence of VOCs, NO rapidly regenerates NO₂ due to the strong oxidizing properties of O₃, resulting in a steady-state cycle. However, the VOCs present in the actual atmosphere can oxidize NO to NO₂, preventing O₃ from undergoing a strong oxidizing reaction with NO and causing O₃ to accumulate continuously (Steinfeld, 1998). Therefore, there is a nonlinear relationship between the degree of O₃ pollution and the levels of NO_x and VOCs. Controlling the emission reduction ratio of both NO_x and VOCs based on the O₃ sensitivity coefficient critically impacts the change in the O₃ concentration in urban areas (Du et al., 2022).

Although conventional back-trajectory cluster analysis (Brankov et al., 1998) and O₃ source apportionment techniques (Li et al., 2013) can infer the potential source regions and emission source types of O₃, they cannot provide the contribution rates of different regions or the specific concentration distributions and contributions of different emission sources. The brute-force method (BFM) can determine the contribution rate of a target emission source by setting all emissions, except for the target, to zero (Wang et al., 2014). However, this approach is computationally demanding for large-scale studies and does not consider the nonlinear impacts among different pollution sources (Wang et al., 2010). The integrated source apportionment module model (CMAQ-ISAM) uses the emission inventory, which cooperates with the physical and chemical transport calculation module inside the model to perform source apportionment on the target pollutants in the form of labels, and obtains their spatiotemporal distribution characteristics, contribution rates and reaction process rates. Wang et al. (2023b) used CMAQ to simulate O₃, NO_x and VOCs in the Pearl River Delta region and concluded that the local emission contribution of VOCs is much greater than that of NO_x and O₃, both of which have strong transport capabilities. Zhang et al. (2023) used the integrated reaction rate module (IPR) in CMAQ to analyze the source and formation mechanism of O₃ and its precursors in the Beijing-Tianjin-Hebei region and concluded that the boundary conditions (BCONs) and local emission contributions were similar and that vertical diffusion during the day led to an increase in the near-surface O₃ concentration.

Chengdu is in the western Sichuan Basin and is one of the largest cities in southwestern China. Due to the proximity of the Qinghai-Tibet Plateau in western Chengdu, the Longquan Mountains in the east, and the mountainous terrain in the north and south, Chengdu is prone to serious O₃ pollution events in summer (Tan et al., 2018). In the summer of 2016 (July August) in Chengdu, O₃ caused severe pollution for 27 days, and the average maximum 8-h concentration reached 322 µg/m³ (Tan et al., 2020). The peak net O₃ production in the four major urban areas of Chengdu in the autumn of the same year was 20–28 ppbv/h (Tan et al., 2018). Related studies have analyzed O₃ pollution in Chengdu and its surrounding counties in the Sichuan Basin area (Du et al., 2022; Lei et al., 2023; Yang et al., 2020). The results showed that the degree and contribution of O₃ pollution in Chengdu were significantly greater than those of the remaining Sichuan Basin (Lei et al., 2023); currently, O₃ simulation analysis research within Chengdu is relatively limited.

Existing research mainly focused on O₃ pollution in the entire Sichuan Basin. There are few studies on the simulation, source analysis and process analysis of O₃ pollution in Chengdu at the urban scale (Du et al., 2022; Wang et al., 2024; Yang et al., 2021). Research summarizing the characteristics of O₃ pollution in Chengdu and providing a basis for the formulation of relevant

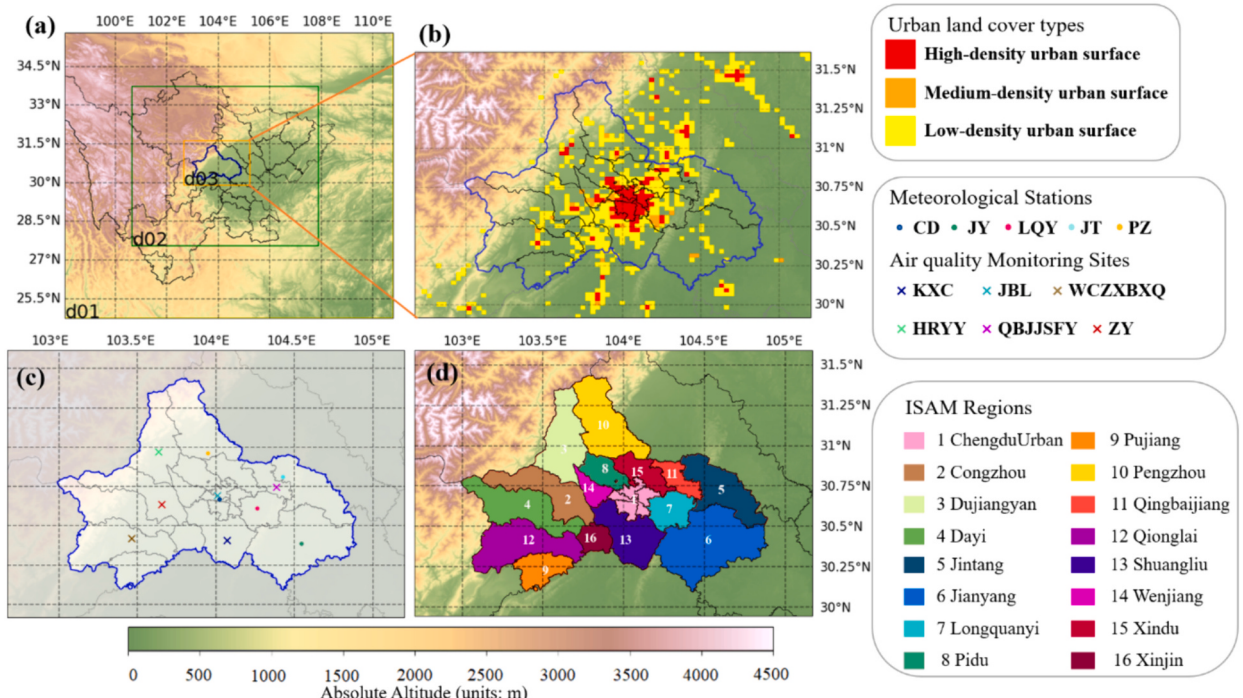


Fig. 1. WRF-CMAQ simulation area. (a) simulation domain, (b) spatial distribution of the urban building density of Chengdu, (c) distribution of meteorological and air quality monitoring sites, (d) Chengdu's 16 districts and counties delineated for the ISAM region setting.

environmental protection policies are needed. In this study, we simulated the meteorological field in Chengdu based on the weather research and forecasting model considering the urban canopy model (WRF-UCM), and jointly used the CMAQ-ISAM model and IPR module to analyze the regional transport source and formation mechanism of O₃ and its precursors under the influence of major anthropogenic and biological source emissions in various districts, counties and urban areas of Chengdu. In [Section 2](#), the configuration of the model, the introduction of each module, and two source resolution scenarios are briefly described. In [Section 3](#), the spatiotemporal distribution of regional emissions, the contribution rates of emission sources in the two scenarios and the process analysis between different transport mechanisms are analyzed. Finally, conclusions are made in [Section 4](#).

2. Data and methods

2.1. WRF-CMAQ model configuration

We used WRFv4.1.2 ([Skamarock et al., 2019](#)) to simulate meteorological conditions and the community multiscale air quality model (CMAQv5.3.2) to simulate O₃ concentrations in Chengdu city. The integrated source apportionment module (ISAM) was applied to analyze the spatiotemporal distribution and regional emission contributions of O₃ and its precursors (VOCs and NO_x), while the integrated process rate module (IPR) was used to determine the rate of change in O₃ during the chemical-physical simulation process. The simulation period is from March 1 to August 31, 2022, predominantly includes the spring and summer seasons in 2022, which roughly represents the duration of this year's warm season. As a period prone to O₃ pollution, Chengdu has experienced multiple heavy O₃ pollution events in the spring and summer of 2022. Among them, a serious O₃ pollution event occurred in August 2022. During this event, the O₃ concentrations exceeded the daily maximum 8-h average (MDA8) limit (165 µg/m³) of the Chinese Ambient Air Quality Standard (GB 3095–2012) for about 20 days. The WRF model has three nested layers, as shown in [Fig. 1](#). The outermost layer, d01, has a spatial resolution of 27 km × 27 km, while the inner two layers, d02 and d03, have spatial resolutions of 9 km × 9 km and 3 km × 3 km, respectively. Among them, d03 covers the entire range of Chengdu. The vertical layer distributions of WRF and CMAQ are consistent, and there are 35 σ layers from the surface to the tropopause. To optimize the simulation results of the meteorological variables in the Chengdu area and increase the accuracy of the O₃ concentration simulations, the WRF model was run with the BEM urban canopy model (a multilayer urban canopy model combined with air-conditioning systems). The WRF model parameterization method and the gas phase chemical mechanism and aerosol chemical mechanism used by CMAQ are shown in [Table 1](#).

2.2. Input data and data processing method

The WRF input data were the 0.25° × 0.25° FNL global reanalysis data provided by the US National Environmental Prediction Center (NECP), and the simulation results were used as the initial conditions (ICONS) and BCONs of the meteorological field required by CMAQ. The default underlying surface data in WRF were constructed for 2000, which is significantly different from the current underlying surface results for Chengdu. To reduce the simulation bias caused by it, we used the 2020 MODIS global 500 m resolution land use product. To meet the requirements of the BEM canopy model in WRF for the division of high-density, medium-density and low-density urban surfaces, we use a 3*3 window based on the MODIS land use product to count the proportion of urban surface, taking 50% and 80% as the boundaries, the urban surface of the three densities are divided, as shown in [Fig. 1b](#).

For the emission inventory of the simulated area, the emissions from anthropogenic sources came from the China Multiscale Emission Inventory Model (MEIC) with a resolution of 0.25° × 0.25° developed by Tsinghua University ([Zheng et al., 2018](#)), and its 2020 emission inventory was used. We utilized the emission inventory allocation tool developed by [Wang et al. \(2023a\)](#) to process the 2020 MEIC emission inventory across four sectors: transportation, residential, industrial, and power sources. The data of road distribution, population density, and industrial area distribution data were used to perform spatial allocation into the CMAQ model's grid; the emissions from natural sources were calculated by MEGANv2.1 ([Guenther et al., 2012](#)). Finally, the emission inventory we obtained for CMAQ simulations contains two spatial resolutions: the resolution of the outermost layer (d01) is 27 km, and that of the innermost layer (d03) is 3 km. The simulated pollutant concentrations of d01 are used as the BCONs and ICONs of d01 to ensure that the external transport can be captured by the model.

Table 1
WRF and CMAQ modeling configurations.

Model	Model attribution	Configuration
WRF	Microphysics	WSM3 (Hong et al., 2004)
	Shortwave radiation	RRTM (Mlawer et al., 1997)
	Longwave radiation	Dudhia (Dudhia, 1989)
	Surface layer physics	Revised MMS Monin-Obukhov
	Land surface model	Noah Land Surface Model (Ek et al., 2003)
	PBL physics scheme	MYJ (Janjić, 1994)
	Cumulus Parameterization	Kain-Fritsch (Kain, 2004)
	Urban canopy model	BEM
CMAQ	Gas-phase chemistry	CB06(Yarwood et al., 2010)
	Aerosol module	AERO6(Murphy et al., 2017 ; Pye et al., 2017)

2.3. ISAM module and configuration

The integrated source apportionment method (ISAM) is a tagging-based source apportionment method commonly used in conjunction with CMAQ. It is widely applied to track different pollutant sources, particularly those with primary and secondary pollutants. The tagged species are incorporated into the chemical transport module for atmospheric chemical and physical process calculations. Kwok et al. (2015) applied ISAM to simulate the contributions of nine source categories to O₃ concentrations in California and compared the results with the brute-force method. They found that the source apportionment results, except for biogenic sources, from both methods had a correlation of >0.9.

ISAM uses two tagging methods: regional tagging and emission source tagging. When the various types of tagged emission pollutants enter the chemical transport mode, under the dominance of chemical mechanisms, some of pollutants from varied tagged categories act as reactants to produce O₃, with varying concentration proportions. Consequently, tagged emission sources can be considered as a source of O₃, despite O₃ not being the primary pollutant. In this study, we tracked the regional emissions from 15 districts of Chengdu city and the high-density urban area of Chengdu (CDurban, comprising the Qingyang, Chenghua, Wuhou, Jinjiang, and Jinniu districts), as shown in Fig. 1d. The final O₃ emissions inventory included both anthropogenic and biogenic sources, with anthropogenic sources consisting of five categories: industrial, power, residential, and transportation. O₃ source apportionment analysis was divided into two scenarios based on two tagging methods: (1) without distinguishing the types of emission sources, all regions were tagged, and each region contained all five types of emission sources; (2) without distinguishing the emission regions, the five different types of emission sources were tagged separately. In addition, the BCONs, ICONs, and untagged emissions (OTHR) that drive the CMAQ simulation process were automatically tagged as supplementary contributions to the simulation results. BCONs mostly include global background values and long-range transport contributions from emission sources outside the simulation area (Kitagawa et al., 2021; Zhang et al., 2023). In this study, the BCONs of d03 is obtained from the simulation results of d01 and mainly represents the contribution of external pollutant transport to d03. The OTHR includes default emission sources in the model that are not explicitly tagged.

2.4. Process analysis module

To understand the mechanism of O₃ formation in Chengdu city during summer, the integrated process rate (IPR) module (Gipson, 1999), embedded in CMAQ, was used in this simulation. In general, in CMAQ simulations, after the atmospheric physical and chemical transport modules have been calculated, only the concentration information of the target species can be obtained. The IPR provides detailed change information during the model prediction process. In this study, seven major physical and chemical processes were chosen for analysis, namely, vertical advection (ZADV), horizontal advection (HADV), horizontal diffusion (HDIF), vertical diffusion (VDIF), dry deposition (DDEP), cloud processes (CLDS) and chemical processes (CHEM), on the overall impact of O₃ and the net change rate of its precursors (Xing et al., 2017).

In the analysis of the IPR results, the reaction processes of different regions near the ground were first examined. The process change rates of the 16 emission locations for O₃ were statistically averaged on a monthly hourly basis to obtain the daily average changes in O₃ for each region, thereby analyzing the characteristics of O₃ formation in each region. Additionally, the daytime and nighttime change rates of each process for O₃ in each layer between 150 and 2500 m were analyzed in each region, and the diurnal variation of O₃ above the near-surface and its impact on the ground level were investigated.

2.5. Site description and model validation methods

In this study, the meteorological variables and O₃ concentrations of WRF and CMAQ were verified using the hourly observation data from meteorological stations and environmental monitoring stations in Chengdu in August 2022. Meteorological observation data were obtained from five different districts in Chengdu city, including Chengdu (CD), Jianyang (JY), Longquanyi (LQY), Pengzhou (PZ), and Jintang (JT). O₃ data from air monitoring stations were obtained from six sites in several counties and districts of Chengdu city, as shown in Fig. 1c. These environmental stations are evenly distributed within Chengdu city. The Jinbo Road (JBL) station in the Jinniu district is a typical urban site, the Science City (KXC) station is in the southern Shuangliu district, the Qingbaijiang Technician College (QBJJSFY) station is in the campus environment of the eastern Qingbaijiang district, and the stations in the western part of Chengdu city are Hairong Pharmaceutical (HRYY), Wenchang Middle School North Campus (WCZXBQ), and Ziyuan (ZY), located in Dujiangyan (DJY), Qionglai (QL), and Chongzhou (CZ), respectively.

The statistical parameters used to evaluate the simulation performance included the mean absolute error (MAE, Eq. 1), correlation coefficient (R), normalized mean error (NME, Eq. 2), normalized mean bias (NMB, Eq. 3), mean fractional error (MFE, Eq. 4), and mean fractional bias (MFB, Eq. 5), where P represents the simulated value and O represents the observed value. According to Boylan and Russell (2006), when $|MFB| \leq 60\%$ and $|MFE| \leq 75\%$, the model results were within an acceptable range of error. When $|MFB| \leq 30\%$ and $|MFE| \leq 50\%$, the simulation performance was good.

$$MAE = \frac{1}{N} \sum_{i=1}^N |P_i - O_i| \quad (1)$$

$$NME = \frac{\sum_i^N |P_i - O_i|}{\sum_i^N O_i} \quad (2)$$

$$NMB = \frac{\sum_i^N (P_i - O_i)}{\sum_i^N O_i} \quad (3)$$

$$MFE = \frac{1}{N} \sum_{i=1}^N \frac{|P_i - O_i|}{(O_i + P_i/2)} \quad (4)$$

$$MFB = \frac{1}{N} \sum_{i=1}^N \frac{(P_i - O_i)}{(O_i + P_i/2)} \quad (5)$$

3. Results and discussion

3.1. Model performance evaluation

The verification results between the meteorological variables simulated by WRF and the observed data from the meteorological stations are shown in Fig. S1 and Table 2. The verification was performed using daily averages from March to August. The correlation coefficients for temperature (T2) at the five stations were relatively good (from 0.95 to 0.97). However, due to the uncertainty of the atmospheric dynamics and physical boundary layer parameterization schemes employed by the model in simulating wind fields in the complex terrain of Chengdu (Hallar et al., 2021), the correlation coefficients for wind speed (WS) were relatively low (from 0.59 to 0.75), with an MAE of approximately 1 m/s. Considering the values of the error parameters (NME, NMB, MFE, and MFB) for both meteorological variables, the simulation accuracy of the meteorological field was within an acceptable range. The verification results of the CMAQ-simulated MDA8 O₃ concentration and observation data of six environmental stations in Chengdu are shown in Table 2, and the observed and simulated values of O₃ concentration from March 1 to August 31 are shown in Fig. S2. The correlation coefficients (from 0.63 to 0.74) for all sites demonstrated a good correlation. Additionally, |MFB| ≤ 30% and |MFE| ≤ 30% indicated that the accuracy of the O₃ concentration simulation was satisfactory. The KXC site located in Shuangliu District in southern Chengdu has a higher MAE (31.12 µg/m³), the MAEs for other stations ranged from 17.22 to 21.52 µg/m³, indicating relatively larger errors at the urban stations, which may have been attributed to certain inaccuracies in the WRF model simulations of the meteorological conditions, impacting the concentration field distribution. Other factors contributing to the uncertainties in the calculation results for Chengdu especially the Shuangliu region, include the selected chemical mechanism, errors in emission inventories, and uncertainties in their distribution (Ou et al., 2016). The commonly used chemical mechanisms in the CMAQ model for simulating O₃ concentrations include CB06, SAPRC99, SAPRC07, and RACM2. Variations in their respective VOC emission inventory methodologies (e.g., CB06 accounts for carbon bond numbers when quantifying VOC emissions, resulting in comparatively higher emissions of PAR relative to other chemical mechanisms) can affect VOC and consequently O₃ concentration simulations. Additionally, differences in the chemical reaction

Table 2
Verification of simulation results.

Model	Station name	Validated parameter	MAE	R	NMB	NME	MFE	MFB
WRF	CD	T2	2.08	0.95	6.5%	8.63%	5.76%	4.04%
		WS	0.51	0.60	-16.34%	23.76%	15.49%	-9.91%
	JY	T2	1.41	0.96	0.52%	5.82%	6.47%	7.83%
		WS	1.36	0.75	-50.13%	50.21%	38.28%	-38.17%
	LQY	T2	1.94	0.97	-6.23%	7.93%	5.37%	-3.78%
		WS	1.42	0.66	-51.25%	51.34%	39.65%	-39.47%
	PZ	T2	1.97	0.96	-6.21%	8.18%	5.76%	-4.01%
		WS	1.41	0.59	-57.65%	57.65%	46.87%	46.87%
	JT	T2	2.01	0.80	-1.76%	6.93%	4.45%	-0.79%
		WS	1.35	0.59	-47.75%	48.02%	37.16%	-36.76%
CMAQ	WCZXBQ		21.52	0.65	-16.03%	26.26%	20.02%	-12.20%
	HRYY		20.81	0.74	-10.76%	23.65%	17.40%	-8.88%
	ZY	O ₃ concentration	17.23	0.73	3.74%	22.67%	16.13%	2.18%
			17.22	0.63	-11.71%	22.35%	16.21%	-7.87%
	KXC		31.12	0.65	-36.70%	37.41%	28.72%	-27.89%
	JBL		18.40	0.69	-11.91%	24.51%	18.32%	-7.46%

intensities among these mechanisms can result in varying simulation errors, particularly due to the reactions of HO₂-NO, RO₂-NO, and the decomposition of NO₂ (Kitayama et al., 2019). According to the spatial distribution of the stations in the Chengdu area, it can be deduced that the average values of all verification parameters of the three sites in the western Chengdu (WCZBXQ, HRYY, ZY) outside the high-density urban area are greater than those of the three sites in central Chengdu and surrounding urban areas. The reason was that under urban area conditions, the model could not accurately simulate the environmental characteristics of the urban area where the sites were located, which led to errors in meteorological variables and subsequently affected the calculation results of the CMAQ chemical process (Zhang et al., 2007). Overall, the simulated O₃ concentration had a relatively high correlation with the observed concentration at the stations, which was similar to the results of previous meteorological and environmental simulation studies conducted in Chengdu (Wang et al., 2021).

3.2. Spatial distribution characteristics of temperature, O₃, and its precursors

Before analyzing the sources of O₃ pollution in Chengdu, it was necessary to first understand the spatial distribution characteristics of the meteorological environment field during the warm season of 2022, as shown in Fig. 2, for the corresponding simulation results. The northwestern area adjacent to the Western Sichuan Plateau features complex terrain and lower atmospheric stability, with variable wind directions and higher wind speeds compared to those of the plains. In contrast, due to the unique topography of the Sichuan Basin (Fig. 1), the plain areas experience low-speed northeasterly winds, the urban areas affected by buildings exhibit the lowest wind speeds, and the wind speeds are higher in the JY and JT regions. Except for the mountainous areas in western Sichuan adjacent to the Qinghai-Tibet Plateau in the west, during the warm season of 2022, Chengdu experienced an average temperature ranging from 19 to 25 °C (Fig. 2a) with a uniform spatial distribution, and the influence of some O₃ pollution chemical processes was strengthened. The seasonal average MDA8 O₃ concentration in Chengdu from March to August 2022 is shown in Fig. 2b. The western districts and counties of Chengdu had a relatively high O₃ concentrations, ranging from 250 to 350 µg/m³. The Pidu (PD) and Wenjiang (WJ) areas in the western main urban area had the highest MDA8 O₃ concentrations, while the eastern districts and counties had relatively lower MDA8 O₃ concentrations. The concentration in the urban area was the lowest. This spatial distribution of O₃ was consistent with the simulation results obtained by Liu et al. (2020) for the summer of 2017. The distributions and concentration differences of O₃ between spring and summer are shown in Fig. S3. The highest MDA8 O₃ concentrations in spring were lower than those in summer, with a more pronounced east-west discrepancy. High concentration areas shift from DJY in spring to XD and PD in summer, with an overall increase ranging from 40 to 120 µg/m³, and a greater increase in urban areas.

The seasonal average distributions of VOCs and NO_x are illustrated in Fig. 2c and Fig. 2d, respectively. In the MEIC emission source inventory, the main urban area of Chengdu is the main emission area of VOCs and NO_x, and the simulation results also show that the main urban area of Chengdu is an area with high concentrations of VOCs and NO_x. However, outside the main urban area of Chengdu, there are differences in concentration levels between the two, which is mainly due to biological VOCs (BVOCs). According to Zhang et al. (2022), the emission intensity of BVOCs at the edge of the Sichuan Basin is relatively high, and due to the advection of BVOCs by

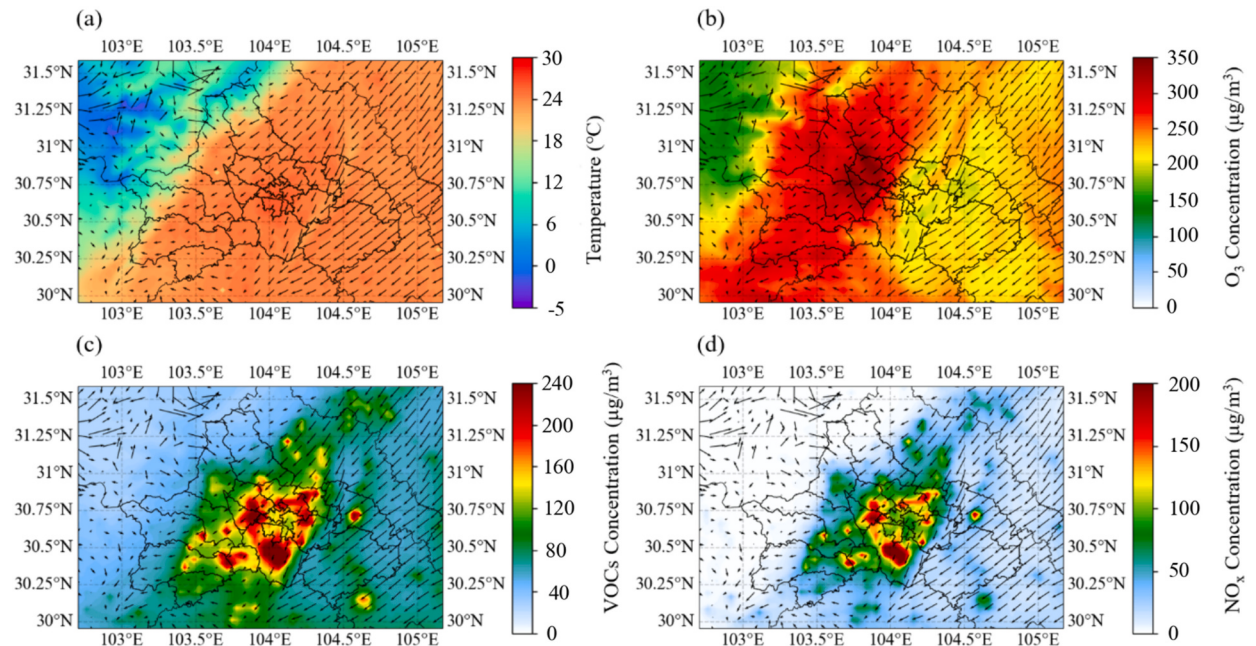


Fig. 2. Seasonal mean values of the meteorological environment in Chengdu from March to August 2022: (a) temperature, (b) MDA8 of O₃ concentrations, (c) VOCs concentrations, and (d) NO_x concentrations, with arrows in the figure indicating the wind direction.

prevailing winds to the downwind area of Chengdu, the concentration of VOCs in the eastern and western regions outside the urban area is greater than that of NO_x.

3.3. O₃ source apportionment of regions in the Chengdu area

According to the setup of the source apportionment scenario (1), the spatial distribution characteristics of the seasonal MDA8 O₃ concentration and wind field during the warm season of 2022 for the 16 tagged districts in Chengdu are shown in Fig. S4. The initial concentration for each tagged area was ranged from 40 to 70 µg/m³. The distribution of O₃ originated from all regions was generally a high-value area in the tagged area, and it spread to the west of Chengdu along the direction of the wind field starting from the tagged area and began to accumulate after reaching the mountainous area in the west, eventually forming the characteristic of high O₃ concentrations in the west and low concentrations in the east (Fig. 2b). The O₃ transport in different tagged areas had different distribution ranges due to the influence of the local environment and wind field and was generally positively related to the local concentration. CDurban, DJY, and LQY had relatively high local emissions among all regions. The CDurban and western districts and counties (DJY, PD, SL, and WJ) had relatively high local emissions among all regions, so their impacts on long-distance transport to other regions were relatively low compared to those on local emissions. CDurban, PD, SL, and WJ are in urban areas where anthropogenic emissions are dominant, in the center of Chengdu, so they are the major regional sources of pollution for their adjacent areas. Due to the persistent northeasterly wind, the O₃ distribution trajectories from each region showed a southwestward spread, resulting in similar characteristics to those of the DJY, with less diffusion and transport to other districts, such as the QL and PJ, in southwestern Chengdu. In contrast, the QBJ, LQY, PZ, XD, and XJ regions had more significant southwestward diffusion effects due to the influence of the wind field, which was one of the important reasons for the high O₃ pollution in the west. Located in the easternmost part of Chengdu, JY and JT are situated on the eastern side of the Longquan Mountains. The higher wind speeds in these areas accelerate the transport of O₃, resulting in a situation where the external O₃ concentration is higher than the local O₃ concentration and blocking part of the O₃ transport to the main urban area.

To quantitatively evaluate the regional sources of O₃ and its precursors, VOCs and NO_x, Fig. 3 shows the seasonal mean contribution rates of each substance in each region. Fig. 4 shows the daily contribution rates of local and other regional emissions to CDurban. In addition to the contribution rate of the marked area, the contribution rates of the ISAM's default BCONs, ICONs, and OTHR

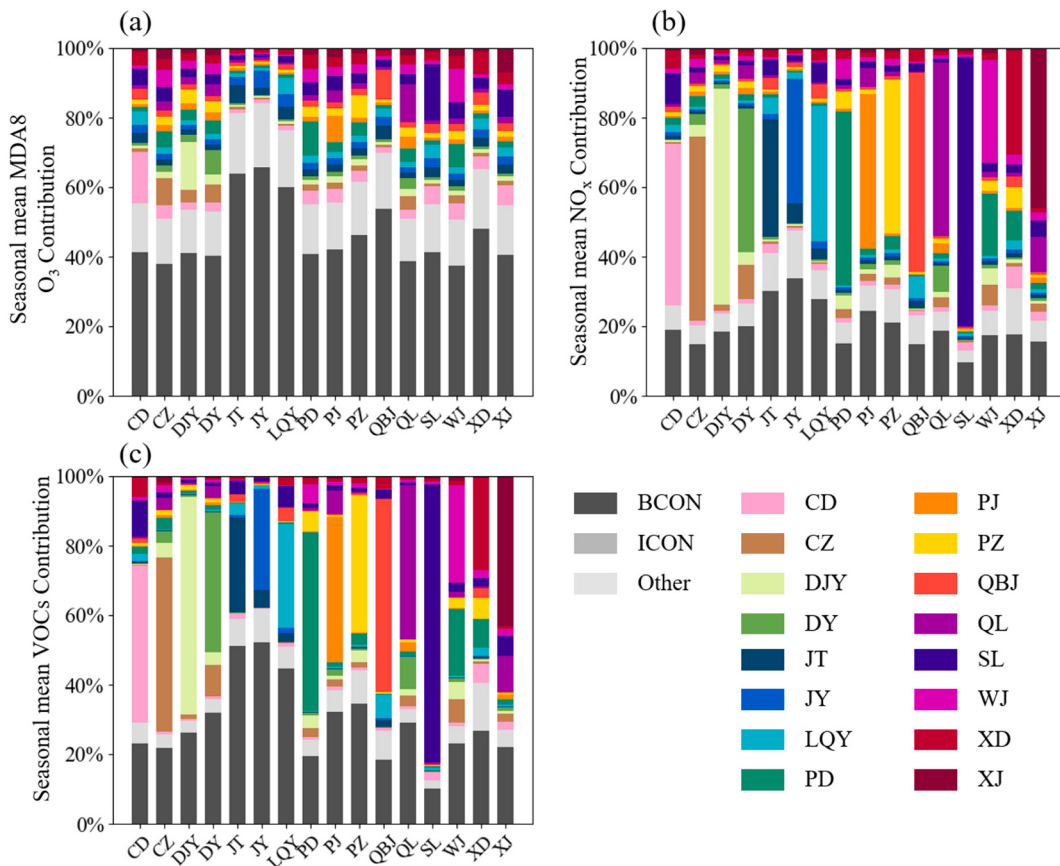


Fig. 3. Seasonal mean contribution rates of O₃, VOCs, and NO_x, to the 16 tagged regions in Chengdu under the regional source apportionment scenario.

involved in the distribution and transport calculations were also determined. From the results of the seasonal contribution calculations for each region, the contribution of BCONs was one of the major sources of O_3 in each region, with a contribution rate ranging from 37.4% to 65.7%, which is consistent with the relevant analysis results of O_3 sources during the warm season in urban areas (Zhang et al., 2023; Zhao et al., 2022). The regional pollution characteristics of O_3 were evident. The local emission contributions of western counties, such as CZ, DY, PJ, and XJ, were much smaller than the transport contributions from other regions. Since the BCONs are generated through the d01 pollution concentration results, the eastern counties JT, JY, and LQY are susceptible to the transport of O_3 originating from outside Chengdu, and their boundary condition contributions are significantly greater than those of other regions. CDurban, DJY, PD, SL, QL, and WJ are in the central and western regions of Chengdu, and their pollution characteristics were similar in terms of local emissions and transport contributions from other regions. The results in Fig. S4 show that the continuous easterly wind in the Sichuan Basin was the main reason for the gradual increase in O_3 pollution in Chengdu from east to west. In areas dominated by local emissions, the local contribution rate to O_3 was greater in summer than in spring (Fig. S5).

For the seasonal average contributions of NO_x and VOCs across regions (Fig. 3b and Fig. 3c), compared with the local emission contributions of O_3 in each region, the local emission contributions of NO_x were significantly greater. Correspondingly, the contribution rates of BCONs decreased in each region. The BCONs contribution rates of both substances exhibit east-west regional disparities, with significant local emission contributions in counties surrounding main urban areas (PD, QBJ, SL). The BCONs contribution rate of VOCs is elevated due to the greater transport of biogenic VOCs (BVOCs) compared to NO_x in all regions.

For the daily average pollution contribution rates of CDurban (Fig. 4), there were differences in the daily average contributions of local emissions, other regional emissions and BCONs throughout the warm season. The difference in the daily average contribution rate of BCONs was the most obvious (ranging from a maximum of 78.2% to a minimum of 9.3%), which was likely due to daily meteorological field changes. In terms of the contributions of the surrounding districts and counties to CDurban, the areas with high contribution rates included LQY, XD, QBJ, and SL. These areas are geographically adjacent to or located in the northeast of CDurban, so O_3 spreads to the southwest to CDurban due to the wind field. Among them, SL has become the main source area of CDurban due to the concentration of emission sources. There are differences in the impact of regional emissions on CDurban between spring and summer. In the spring, the local emission contribution of CDurban was lower than that in the summer. In summer, there are often consecutive periods when the transport contribution of surrounding areas increases significantly (such as June 26 to July 16 and July 18 to August 15), while there are fewer such periods in spring.

The daily mean contribution rates of NO_x and VOCs from different regional emissions to CDurban, as illustrated in Fig. 4b and Fig. 4c, show that local emissions remain the dominant source, followed by contributions from BCONs and external regional transport. The daily average contributions of the boundary sources of NO_x and VOCs differ slightly in spring. However, due to the increase in and transport of BVOC emissions over the Sichuan Basin in summer (Zhang et al., 2022), the boundary contribution of VOCs in summer is greater than that of NO_x . For regional sources of NO_x and VOCs, SL and XD had relatively large impacts on CDurban. It is noted that they are also O_3 regional sources of CDurban.

Overall, BCONs are a significant source of O_3 pollution in Chengdu during the warm season, indicating that the transport impact

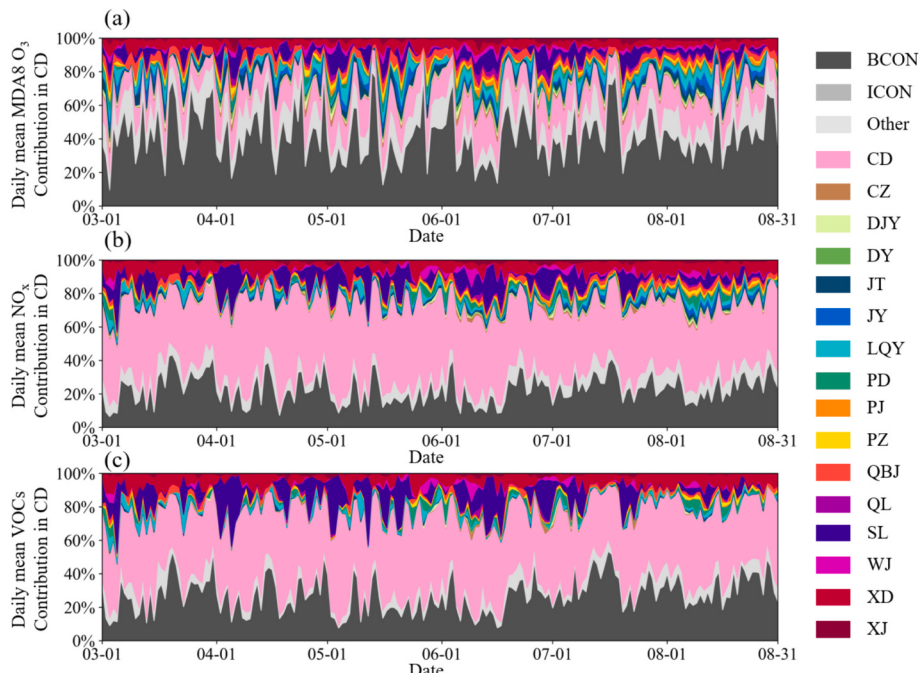


Fig. 4. Daily mean contribution rates of MDA8 O_3 , VOCs, and NO_x to CDurban under the regional source apportionment scenario.

from long-distance areas outside the city is one of the factors that should be considered during O₃ control. CDurban's local emissions have a lower impact on O₃ than precursors, indicating that in addition to CDurban's O₃ being affected by the photochemical reaction of local precursors, regional O₃ transport is also an important factor. The SL and XD areas, which contribute significantly to CDurban's O₃, NO_x and VOCs, should be focused on.

3.4. O₃ source apportionment of emissions in the Chengdu area

Since the simulated O₃ concentration distribution characteristics were closely related to the emission sources, different types of emission sources had varying effects. According to the source apportionment scenario (2), the spatial distributions of the seasonal mean MDA8 O₃ concentrations in Chengdu generated by industrial, residential, power, transportation, and biological sources were shown in Fig. S6. Among them, emissions from residential and power sources peak at relatively low levels (approximately 30 µg/m³), while industrial, transportation, and other sources could reach the highest emission concentrations (80 µg/m³). From the spatial distribution, it could be observed that the O₃ concentration was still higher in the western region than in the eastern region, and emissions from all sources were high in the PD and WJ regions, similarly, due to the transport effect of the wind field, low concentrations were observed in the eastern part of the Longquan Mountains. Regarding the spatial distribution of O₃ concentration caused by each emission source, the high-value area for industrial sources was in certain industrial zones within Chengdu city, with dispersion occurring in the central and western regions. For transportation sources, the high-value area began in CDurban, WJ, and PD and spread westward along the road network in neighboring areas such as DY, PJ and CZ. Since transportation emissions primarily affect the NO_x concentration, the influence of transportation sources on the dispersion of O₃ originates from the chemical reaction of the generated NO_x with VOCs. This influence was further driven by the easterly winds, extending the dispersion to the western region of Chengdu. A high-value distribution of O₃ emissions from biological sources was found in low-density areas of the city, particularly near the western mountainous regions of Sichuan. This indicated that the high vegetation coverage in the western region contributed to BVOCs generation, which was one of the factors increasing O₃ concentrations in the western area.

Fig. 5 presents the seasonal mean contribution rates of the five tagged emission sources to O₃ and its precursors in different districts and counties of Chengdu. The boundary conditions, still represent the total transport contribution of all types of emission sources from the outer simulation area, which is consistent with the regional apportionment scenario. Regarding warm season emission source

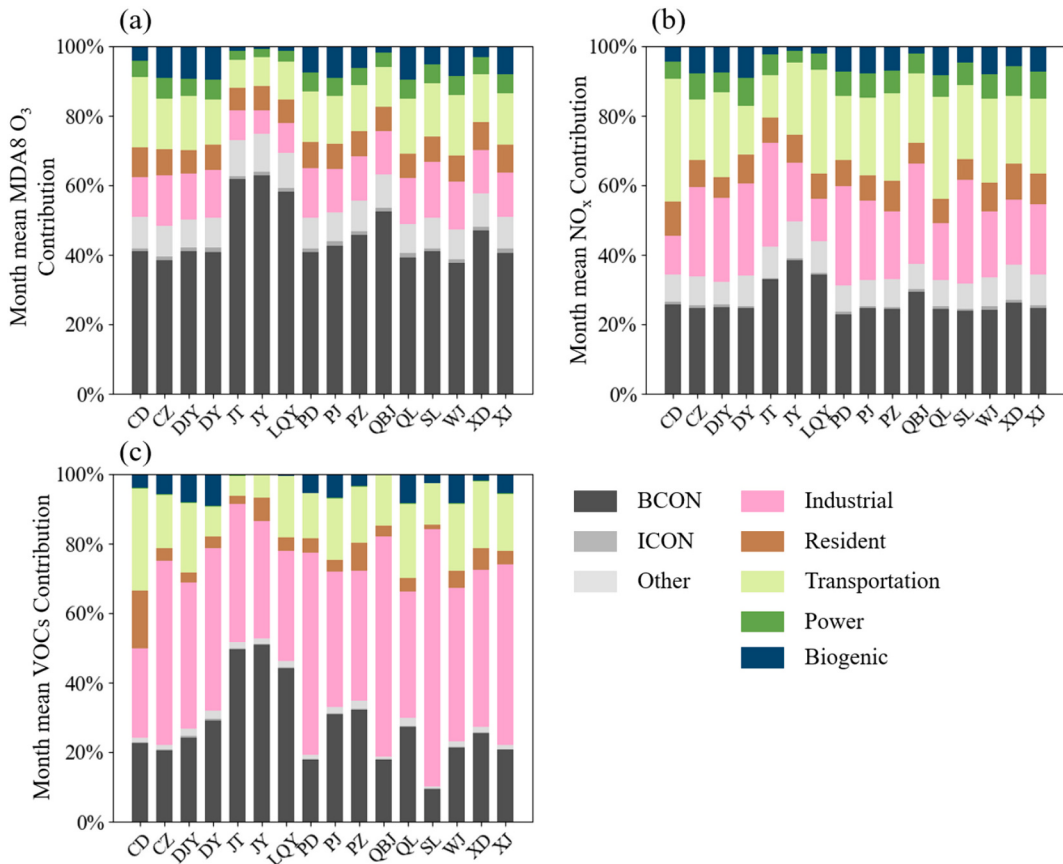


Fig. 5. Seasonal mean contribution rates of O₃, VOCs, and NO_x of the 16 tagged regions in Chengdu under the source apportionment scenario for different emission types.

contributions to O₃ (Fig. 5a), the sources with relatively high contribution rates to the O₃ and NO_x concentrations were transportation, industrial, and biological sources. The contribution rates of the other two anthropogenic sources, residential and power sources, were relatively stable across all regions and had lower contribution rates. Comparing each region, regarding the contribution of O₃, BCONs still accounted for the highest proportion. The contribution of transportation sources in CDurban is greater than that in other regions, while the contribution of biogenic sources in the western districts is relatively higher. Regarding the contribution of NO_x emission sources, the proportion of BCONs is significantly lower than that of O₃, which mainly comes from transportation sources and industrial sources, and transportation sources are generally higher than industrial sources. Excluding CDurban, industrial sources are the primary contributors to VOCs emissions in all regions. The contribution of biological sources is relatively obvious in the western and central districts and counties, indicating that in addition to externally transmitted BVOCs, areas with dense vegetation in the west are the main local sources of BVOCs emissions in Chengdu.

For the daily emission source contribution rates in CDurban (Fig. 6(a)-(c)), except for high BCON days, the main emission sources (transportation, industrial, and residential) of O₃, NO_x and VOCs show no significant daily contribution differences in spring and summer. However, the contribution of biogenic sources clearly increase during summer, which is directly correlated with the rise in BVOC emissions reported by MEGAN (Zhang et al., 2022).

Although boundary conditions have a greater contribution to Chengdu's O₃ concentration, they are difficult to control. We should focus on O₃ precursor emissions from traffic sources and industrial sources in Chengdu, and formulate corresponding emission reduction measures to reduce O₃ concentrations.

3.5. Atmospheric process contributions to O₃ in the Chengdu area

To further investigate the contributions of seven different physical and chemical processes to O₃ pollution in the 16 regions of Chengdu city, we utilized the CMAQ process analysis tool to calculate the hourly mean changes in warm season O₃ concentration rates at the ground level (50–100 m) for different counties and under different physical and chemical processes.

According to the overall results of each region (Fig. 7), within the scope of Chengdu, the processes important for O₃ concentration variations within Chengdu city were chemical process (CHEM), vertical diffusion (VDIF), horizontal advection (HADV), and dry deposition (DDEP). Among these processes, horizontal advection and vertical diffusion contributed to the increase in O₃ concentrations, while chemical processes and dry deposition primarily acted to remove O₃. The vertical diffusion process significantly impacted the increase in O₃ concentrations in most regions during the period of 10:00 to 18:00, while its influence was weaker during the nighttime period. On the other hand, the horizontal advection process primarily contributed to the increase in O₃ concentrations during the periods from 00:00 to 9:00 and from 19:00 to 23:00. The dry deposition process mainly occurred from 10:00 to 18:00 and contributed to O₃ removal. This phenomenon was related to the daytime boundary layer height and atmospheric stability (Miao et al., 2018). The chemical process significantly contributed to the reduction in near-surface O₃ concentrations and occurred during all

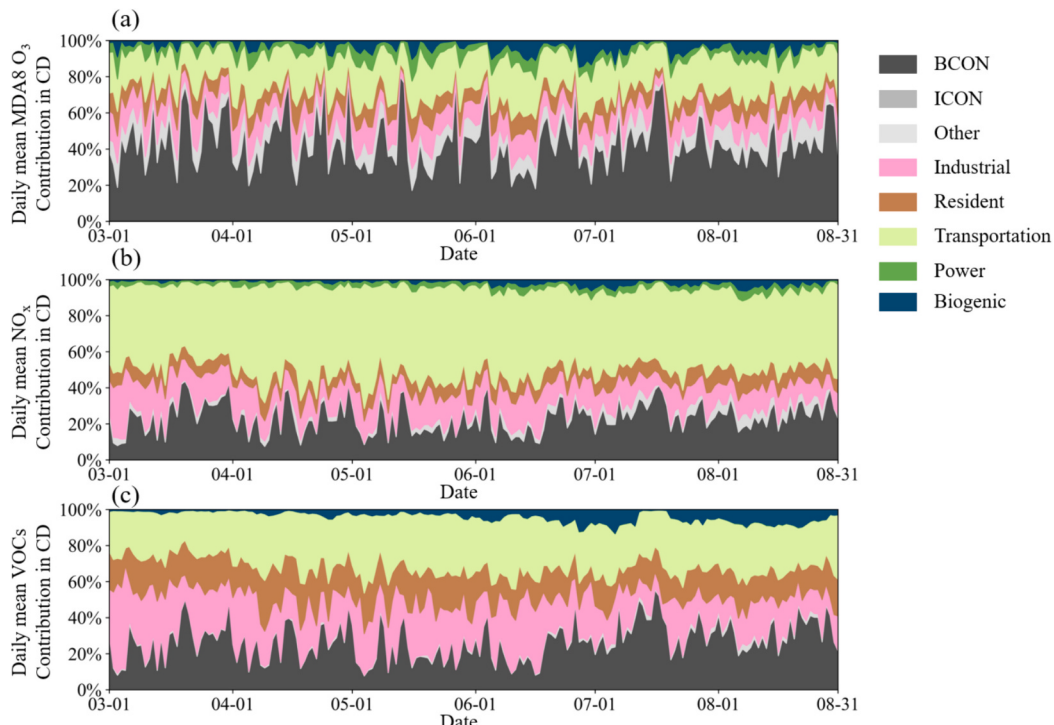


Fig. 6. Daily mean contribution rates of O₃, VOCs, and NO_x to CDurban under the source apportionment scenario for different emission types.

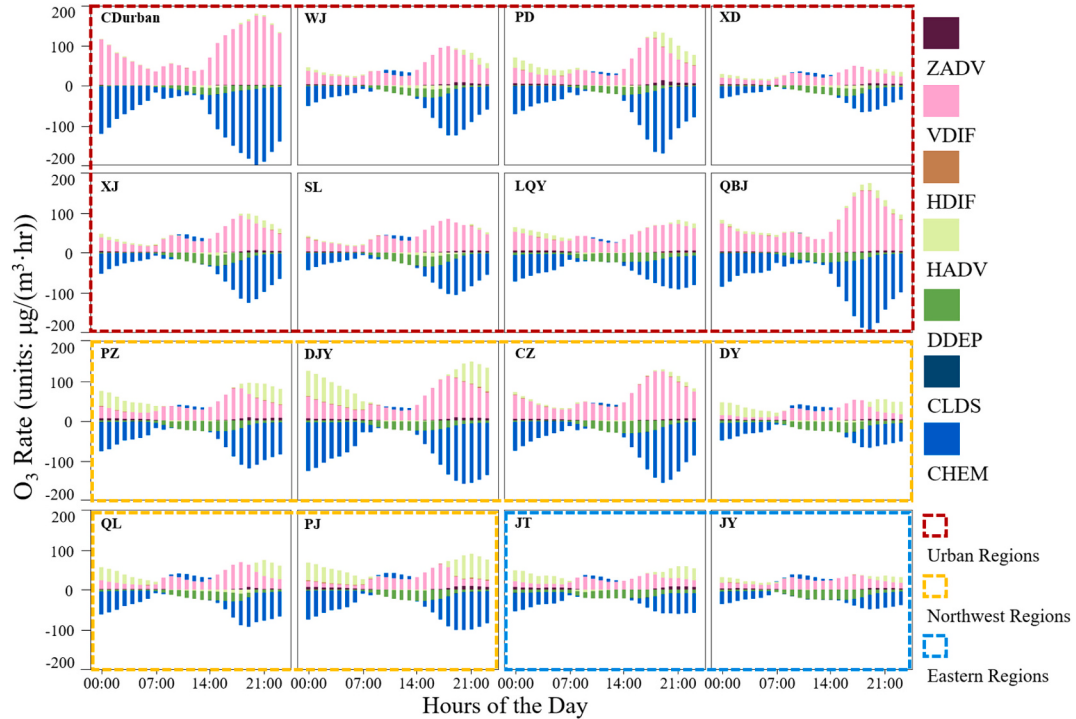


Fig. 7. Monthly mean O_3 process rates per hour in 16 regions of Chengdu near the surface (50–100 m), including vertical advection (ZADV), horizontal advection (HADV), horizontal diffusion (HDIF), vertical diffusion (VDIF), dry deposition (DDEP), cloud physical processes (CLDS), and chemical processes (CHEM).

periods. In most regions, the highest rate of change (from -70 to $-200 \mu\text{g}/(\text{m}^3 \cdot \text{hr})$) was reached starting at 17:00. However, there were also certain regions where positive chemical processes during the daytime contributed to an increase in O_3 concentrations. This could be attributed to the high temperatures and intense sunlight during the daytime period, which led to O_3 generation through photochemical reactions. Furthermore, during the period of frequent motor vehicle traffic starting at 17:00, O_3 underwent titration reactions with a large amount of NO generated by anthropogenic traffic sources, resulting in a depletion of O_3 concentrations (Zaveri, 2003). Outside the heavily trafficked areas, O_3 continued to be transported between regions through horizontal advection, resulting in a combination of local emissions and regional transport that contributed to O_3 pollution in each region.

Due to variations in geographical location, environmental factors, meteorological conditions, regional pollution transport and urban density, different regions exhibit distinct characteristics in terms of the contribution rates of near-surface O_3 transport mechanisms. The analysis divides the area into three categories: eastern (JT, JY), western (CZ, DJY, CZ, DY, QL, PJ), and urban (CDurban, WJ, PD, WD, XJ, SL, LQY, QBJ). For the urban region, the variations in near-surface O_3 are primarily governed by vertical diffusion and chemical processes; during the period of frequent vehicular activity (14:00–21:00), there was a strong vertical diffusion and removal through chemical processes. The chemical removal amounts in CDurban and QBJ both reached the highest values in the entire region ($-200 \mu\text{g}/(\text{m}^3 \cdot \text{hr})$) at night (19:00 and 20:00), and the overall removal amounts were higher than those in the eastern and western regions. This is directly related to the oxidation reaction of high concentrations of NO_x (Fig. 2c) and O_3 in urban areas. (Palmgren et al., 1996). The generation of O_3 by horizontal advection only occurred in XJ, which is located southwest of CDurban, and WJ and PD, which are located in the upwind area west of the Longquan Mountains. For the western region, due to the decrease in urban density, the overall removal amount of O_3 by chemical processes is lower than that in urban areas. Only DJY and CZ had relatively high removal amounts due to the presence of high-density urban areas. Due to the continuous westerly wind field in the warm season, the increasing effect of horizontal advection on O_3 is significantly enhanced in the western region, and the continuous increase occurs from night to 7:00 the next day. The elimination ability of dry deposition also increases slightly due to environmental differences. In southwestern areas (DY, QL, and PJ) with high vegetation coverage, O_3 is chemically generated during the daytime starting at 7:00 due to the emission of BVOCs and the catalytic effect of residual NO_x (Atkinson, 2000). For the eastern region, due to lower local O_3 concentrations, the absolute value of the change is relatively low, but the horizontal advection is also significant due to the wind field. A comparison of the average physical and chemical process change rates in the warm season in each region is shown in Fig. S7. The maximum change rate increases due to the increase in O_3 concentrations in summer, and the intensity of the dry deposition process is also greater than that in spring.

Furthermore, the daytime (07:00–18:00) and nighttime (19:00–07:00) mean change rates of each process in the upper near-surface layer (150–2500 m) of Chengdu are presented in Fig. 8. During the daytime, chemical processes contribute positively to O_3 concentrations at upper levels, and the change rate is greater at 150–1000 m, indicating that this height is the main photochemical

reaction height of O₃ in Chengdu and that the corresponding vertical diffusion plays a negative role in the O₃ concentration. At the same time, there is also a certain negative contribution from horizontal advection. At night, within 150–500 m where the change rate is relatively high, the main positive contribution to O₃ is horizontal advection, while chemical processes make a negative contribution to O₃. This finding is consistent with the conclusion obtained by Zhang et al. (2019) through sounding balloon observations in the urban area of Shanghai. Therefore, photochemical reactions in the boundary layer were the primary source of O₃ in the upper atmosphere. Through the continuous process of vertical diffusion, the upper-level O₃ was transported to the near-surface to compensate for the losses caused by NO titration at night. This resulted in an increased contribution of near-surface vertical diffusion, which was ultimately transported to the urban surface through dry deposition and NO titration (Tang et al., 2017). Additionally, due to the decrease in the rate of increase in the upper-level O₃ concentration and changes in the wind field at night, horizontal advection plays a dominant role in O₃ transport.

The results for each of the three regions are shown in Fig. S8 and Fig. S9. In urban areas, urban heat island circulation in high-density areas complicate meteorological conditions and elevate the boundary layer in urban zones (Mughal et al., 2019), causing the total change rate of photochemical reactions on O₃ concentration during the day and the transport height of horizontal advection at night to be higher than those in non-urban areas. In addition, due to the higher NO_x emissions in urban areas, the intensity of the O₃ titration reaction is stronger at night, especially in CDurban. Since the western region is downwind, the removal rate of horizontal advection is lower than that in urban areas. In the eastern region, due to higher local wind speeds, the removal of horizontal advection and the intensity of vertical advection are greater. For CDurban, the intensity and reaction height of vertical diffusion during both day and night exceed those of other areas. This is due to the formation of a residual layer near the surface caused by radiative cooling after sunset (Stull, 1988). The O₃ present in this residual layer descends and mixes into the newly formed mixed layer during the next day's sunrise (Hu et al., 2013), and coupled with the impact of urban heat islands and building topography on wind speed, CDurban has a greater residual layer and mixed layer, which strengthens the height and intensity of this process (Sarrat et al., 2006).

4. Conclusions

We employed the WRF-CMAQ model, along with source apportionment and process analysis modules, to analyze the O₃ levels, precursor VOCs and NO_x contributions, and formation mechanisms in Chengdu city during warm seasons in 2022. Our work shows that due to the advection transport of the northeasterly wind field, the overall O₃ concentrations in Chengdu exhibit a spatial distribution with high concentrations in the west and low concentrations in the east. The precursors NO_x and VOCs are mainly distributed in urban areas with high concentrations. Regional transport analysis shows that O₃ in Chengdu is mainly influenced by local emissions of NO_x

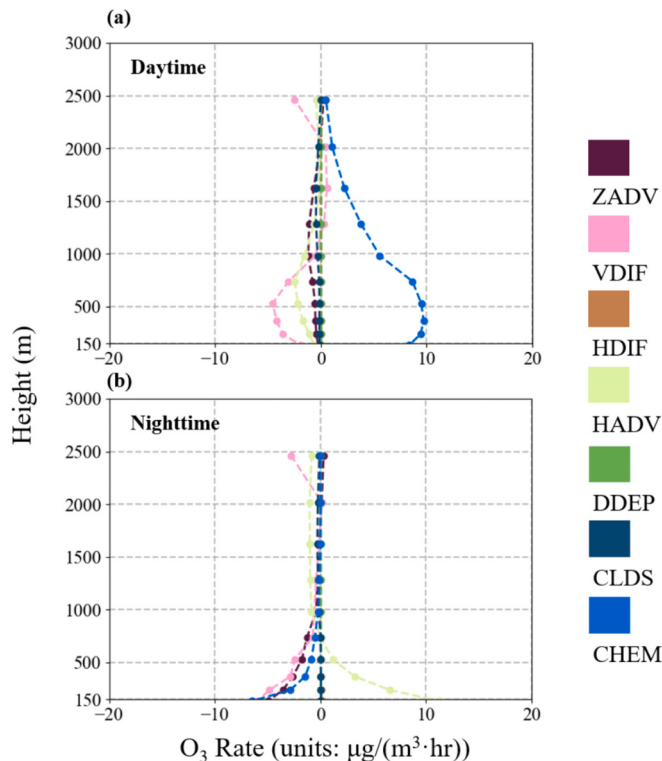


Fig. 8. Monthly mean O₃ process rates in warm season day (07:00–18:00) and night (19:00–07:00) in all areas of Chengdu at different altitudes ranging from 150 to 2500 m.

and VOCs, as well as O₃ transported from outside areas. This leads to varying O₃ levels across regions, largely due to local and boundary sources. It's suggested that high-emitting areas like SL and XD near Chengdu's urban center should control emissions and possibly create a regional plan to manage O₃ transport from afar. The primary sources of O₃ in Chengdu's urban area are the emissions of NO_x from traffic and industrial, and VOCs from residential areas, which together significantly contribute to O₃ concentrations. The contribution of biogenic emissions from BVOCs transported from western Chengdu and the Sichuan Basin will increase in summer. That is, in addition to controllable anthropogenic emissions, biological sources should also be considered for summer O₃ pollution events in Chengdu. According to the process analysis results, O₃ in Chengdu is mainly generated by photochemical reactions in the upper near-surface layer during the daytime, and then mainly diffuses vertically to the near-surface layer. A small part is transported horizontally to other areas under the action of the wind field, and is eliminated through titration reactions at night. At the same time, in urban areas with higher NO_x concentrations, the intensity of photochemical reactions, ozone vertical diffusion, and horizontal advection are greater than those in non-urban areas. It is necessary to pay attention to the daytime sunshine, temperature, and the wind field characteristics at night for the prevention and control of O₃ pollution in Chengdu.

CRediT authorship contribution statement

Yaohan Xian: Writing – review & editing, Writing – original draft, Methodology, Investigation, Formal analysis, Conceptualization. **Yang Zhang:** Writing – review & editing, Project administration, Funding acquisition, Conceptualization. **Zhihong Liu:** Project administration, Conceptualization. **Haofan Wang:** Resources, Data curation, Conceptualization. **Junjie Wang:** Resources, Data curation. **Chao Tang:** Resources, Data curation.

Declaration of competing interest

The authors declare no conflict of interest.

Data availability

Data will be made available on request.

Acknowledgment

This study was supported by the Sichuan Science and Technology Program (2023YFS0383, 2023NSFSC0745), the Chengdu Science and Technology Project (2022-YF05-00770-SN), the Unveiling and Commanding Technology Project of Longquanyi District, Chengdu (2023LQYF0011), the National Natural Science Foundation of China (41901294), and the College Students' Innovative Entrepreneurial Training Plan Program (202310621360, 202210621045, 202210621053).

Appendix A. Supplementary data

Supplementary data to this article can be found online at <https://doi.org/10.1016/j.uclim.2024.102017>.

References

- Arneth, A., Harrison, S.P., Zaehle, S., Tsigaridis, K., Menon, S., Bartlein, P.J., Vesala, T., 2010. Terrestrial biogeochemical feedbacks in the climate system. *Nat. Geosci.* 3 (8), 525–532. <https://doi.org/10.1038/ngeo905>.
- Atkinson, R., 2000. Atmospheric chemistry of VOCs and NOx. *Atmos. Environ.* 34 (12–14), 2063–2101. [https://doi.org/10.1016/s1352-2310\(99\)00460-4](https://doi.org/10.1016/s1352-2310(99)00460-4).
- Boylan, J.W., Russell, A.G.J.A.E., 2006. Pm and light extinction model performance metrics, goals, and criteria for three-dimensional air quality models. *Atmos. Environ.* 40 (26), 4946–4959.
- Brankov, E., Rao, S.T., Porter, P.S., 1998. A trajectory-clustering-correlation methodology for examining the long-range transport of air pollutants. *Atmos. Environ.* 32 (9), 1525–1534. [https://doi.org/10.1016/s1352-2310\(97\)00388-9](https://doi.org/10.1016/s1352-2310(97)00388-9).
- Cohen, A.J., Brauer, M., Burnett, R., Anderson, H.R., Frostad, J., Estep, K., Forouzanfar, M.H., 2017. Estimates and 25-year trends of the global burden of disease attributable to ambient air pollution: an analysis of data from the global burden of diseases study 2015. *Lancet* 389 (10082), 1907–1918. [https://doi.org/10.1016/S0140-6736\(17\)30505-6](https://doi.org/10.1016/S0140-6736(17)30505-6).
- Du, X., Tang, W., Zhang, Z., Li, Y., Yu, Y., Xiao, Z., Meng, F., 2022. Sensitivity modeling of ozone and its precursors over the Chengdu metropolitan area. *Atmos. Environ.* 277 <https://doi.org/10.1016/j.atmosenv.2022.119071>.
- Dudhia, J., 1989. Numerical study of convection observed during the winter monsoon experiment using a mesoscale two-dimensional model. *J. Atmos. Sci.* 46 (20), 3077–3107. [https://doi.org/10.1175/1520-0469\(1989\)046<3077:Nsocod>2.0.Co;2](https://doi.org/10.1175/1520-0469(1989)046<3077:Nsocod>2.0.Co;2).
- Ek, M.B., Mitchell, K.E., Lin, Y., Rogers, E., Grunmann, P., Koren, V., Tarpley, J.D., 2003. Implementation of Noah land surface model advances in the national centers for environmental prediction operational mesoscale eta model. *J. Geophys. Res. Atmos.* 108 (D22) <https://doi.org/10.1029/2002jd003296>.
- Gipson, G., 1999. Chapter 16: process analysis, Science Algorithms of the Epa Models-3 Community Multiscale Air Quality (Cmaq) Modeling System. In: EPA/600/R-99/030.
- Guenther, A.B., Jiang, X., Heald, C.L., Sakulyanontvittaya, T., Duhl, T., Emmons, L.K., Wang, X., 2012. The model of emissions of gases and aerosols from nature version 2.1 (MEGAN2.1): an extended and updated framework for modeling biogenic emissions. *Geosci. Model Dev.* 5 (6), 1471–1492. <https://doi.org/10.5194/gmd-5-1471-2012>.
- Hallar, A.G., Brown, S.S., Crozman, E., Barsanti, K., Cappa, C.D., Faloona, I., Sullivan, A., 2021. Coupled air quality and boundary-layer meteorology in Western U.S. basins during winter: design and rationale for a comprehensive study. *Bull. Am. Meteorol. Soc.* 0, 1–94. <https://doi.org/10.1175/bams-d-20-0017.1>.

- Hong, S.-Y., Dudhia, J., Chen, S.-H., 2004. A revised approach to ice microphysical processes for the bulk parameterization of clouds and precipitation. *Mon. Weather Rev.* 132 (1), 103–120. [https://doi.org/10.1175/1520-0493\(2004\)132<0103:Aratim>2.0.Co;2](https://doi.org/10.1175/1520-0493(2004)132<0103:Aratim>2.0.Co;2).
- Hu, X.-M., Klein, P.M., Xue, M., Zhang, F., Doughty, D.C., Forkel, R., Fuentes, J.D., 2013. Impact of the vertical mixing induced by low-level jets on boundary layer ozone concentration. *Atmos. Environ.* 70, 123–130. <https://doi.org/10.1016/j.atmosenv.2012.12.046>.
- Janjić, Z. I. (1994). The Step-Mountain Eta Coordinate Model: Further Developments of the Convection, Viscous Sublayer, and Turbulence Closure Schemes. *Monthly Weather Review*, 122(5), 927–945. doi:10.1175/1520-0493(1994)122<0927:Tsmecm>2.0.Co;2.
- Kain, J.S., 2004. The Kain–Fritsch convective parameterization: an update. *J. Appl. Meteorol.* 43 (1), 170–181. [https://doi.org/10.1175/1520-0450\(2004\)043<0170:Tkcpau>2.0.Co;2](https://doi.org/10.1175/1520-0450(2004)043<0170:Tkcpau>2.0.Co;2).
- Kitagawa, Y.K.L., Peduzzi, R., Galvão, E.S., de Araújo, I.B., de Albuquerque, T.T.A., Kumar, P., Moreira, D.M., 2021. Source apportionment modelling of PM2.5 using CMAQ-ISAM over tropical coastal-urban area. *Atmospheric. Pollut. Res.* 12 (12) <https://doi.org/10.1016/j.apr.2021.101250>.
- Kitayama, K., Morino, Y., Yamaji, K., Chatani, S., 2019. Uncertainties in O₃ concentrations simulated by CMAQ over Japan using four chemical mechanisms. *Atmos. Environ.* 198, 448–462. <https://doi.org/10.1016/j.atmosenv.2018.11.003>.
- Kwok, R.H.F., Baker, K.R., Napelenok, S.L., Tonnesen, G.S., 2015. Photochemical grid model implementation and application of VOC, NO_x, x, and O₃ source apportionment. *Geosci. Model Dev.* 8 (1), 99–114. <https://doi.org/10.5194/gmd-8-99-2015>.
- Lei, Y., Wu, K., Zhang, X., Kang, P., Du, Y., Yang, F., Hou, J., 2023. Role of meteorology-driven regional transport on O₃ pollution over the Chengdu plain, southwestern China. *Atmos. Res.* 285 <https://doi.org/10.1016/j.atmosres.2023.106619>.
- Li, Y., Lau, A.K.H., Fung, J.C.H., Ma, H., Tse, Y., 2013. Systematic evaluation of ozone control policies using an ozone source apportionment method. *Atmos. Environ.* 76, 136–146. <https://doi.org/10.1016/j.atmosenv.2013.02.033>.
- Li, J., Wang, Y., Qu, H., 2019. Dependence of summertime surface ozone on NO_x and VOC emissions over the United States: peak time and value. *Geophys. Res. Lett.* 46 (6), 3540–3550. <https://doi.org/10.1029/2018gl081823>.
- Liu, H., Deng, Y., Lu, C., Zhang, X., Yang, X., Song, D., Tan, Q., 2020. A CMAQ-based study on evaluation of achievements of measures on ozone pollution prevention and control in summer 2017 in Chengdu. *IOP Conf. Ser.: Earth Environ. Sci.* 610 (1) <https://doi.org/10.1088/1755-1315/610/1/012015>.
- Miao, Y., Liu, S., Guo, J., Huang, S., Yan, Y., Lou, M., 2018. Unraveling the relationships between boundary layer height and PM_{2.5} pollution in China based on four-year radiosonde measurements. *Environ. Pollut.* 243 (Pt B), 1186–1195. <https://doi.org/10.1016/j.envpol.2018.09.070>.
- Mlawer, E.J., Taubman, S.J., Brown, P.D., Iacono, M.J., Clough, S.A., 1997. Radiative transfer for inhomogeneous atmospheres: RRTM, a validated correlated-k model for the longwave. *J. Geophys. Res. Atmos.* 102 (D14), 16663–16682. <https://doi.org/10.1029/97jd00237>.
- Mughal, M.O., Li, X.X., Yin, T., Martilli, A., Brousse, O., Disegna, M.A., Norford, L.K.J.J.O.G.R.A., 2019. High-resolution, multilayer modeling of Singapore's urban climate incorporating local climate zones. *J. Geophys. Res. Atmos.* 124 (14), 7764–7785.
- Murphy, B.N., Woody, M.C., Jimenez, J.L., Carlton, A.M.G., Hayes, P.L., Liu, S., Pye, H.O.T., 2017. Semivolatile POA and parameterized total combustion SOA in CMAQv5.2: impacts on source strength and partitioning. *Atmos. Chem. Phys.* 17, 11107–11133. <https://doi.org/10.5194/acp-17-11107-2017>.
- Ou, J., Yuan, Z., Zheng, J., Huang, Z., Shao, M., Li, Z., Louie, P.K., 2016. Ambient ozone control in a photochemically active region: short-term despiking or long-term attainment? *Environ. Sci. Technol.* 50 (11), 5720–5728. <https://doi.org/10.1021/acs.est.6b00345>.
- Palmgren, F., Berkowicz, R., Hertel, O., Vignati, E., 1996. Effects of reduction of NO_x on the NO₂ levels in urban streets. *Sci. Total Environ.* 189–190, 409–415. [https://doi.org/10.1016/0048-9697\(96\)05238-2](https://doi.org/10.1016/0048-9697(96)05238-2).
- Pye, H.O.T., Murphy, B.N., Xu, L., Ng, N.L., Carlton, A.G., Guo, H., Goldstein, A.H., 2017. On the implications of aerosol liquid water and phase separation for organic aerosol mass. *Atmos. Chem. Phys.* 17 (1), 343–369. <https://doi.org/10.5194/acp-17-343-2017>.
- Sarrat, C., Lemonsu, A., Masson, V., Guedalia, D., 2006. Impact of urban heat island on regional atmospheric pollution. *Atmos. Environ.* 40 (10), 1743–1758. <https://doi.org/10.1016/j.atmosenv.2005.11.037>.
- Skamarock, W.C., Klemp, J.B., Dudhia, J., Gill, D.O., Liu, Z., Berner, J., Barker, D.M.J., N. t. n. n. t-s., 2019. A description of the advanced research WRF version 4, p. 145.
- Steinfeld, J.I., 1998. Atmospheric chemistry and physics: from air pollution to climate change. *Environ. Sci. Policy Sustain. Dev.* 40 (7), 26. <https://doi.org/10.1080/00139157.1999.10544295>.
- Stull, R.B., 1988. *An Introduction to Boundary Layer Meteorology*, 13. Springer Science & Business Media.
- Tan, Z., Lu, K., Jiang, M., Su, R., Dong, H., Zeng, L., Zhang, Y., 2018. Exploring ozone pollution in Chengdu, southwestern China: a case study from radical chemistry to O₃(VOC-NO_x) sensitivity. *Sci. Total Environ.* 636, 775–786. <https://doi.org/10.1016/j.scitotenv.2018.04.286>.
- Tan, Q., Zhou, L., Liu, H., Feng, M., Qiu, Y., Yang, F., Wei, F., 2020. Observation-based summer O₃ control effect evaluation: a case study in Chengdu, a megacity in Sichuan Basin, China. *Atmosphere* 11 (12). <https://doi.org/10.3390/atmos11121278>.
- Tang, G., Zhu, X., Xin, J., Hu, B., Song, T., Sun, Y., Wang, Y., 2017. Modelling study of boundary-layer ozone over northern China - part I: ozone budget in summer. *Atmos. Res.* 187, 128–137. <https://doi.org/10.1016/j.atmosres.2016.10.017>.
- Wang, S., Wei, W., Li, D., Aunan, K., Hao, J., 2010. Air pollutants in rural homes in Guizhou, China – concentrations, speciation, and size distribution. *Atmos. Environ.* 44 (36), 4575–4581. <https://doi.org/10.1016/j.atmosenv.2010.08.013>.
- Wang, L.T., Wei, Z., Yang, J., Zhang, Y., Zhang, F.F., Su, J., Zhang, Q., 2014. The 2013 severe haze over southern Hebei, China: model evaluation, source apportionment, and policy implications. *Atmos. Chem. Phys.* 14 (6), 3151–3173. <https://doi.org/10.5194/acp-14-3151-2014>.
- Wang, H., Liu, Z., Zhang, Y., Yu, Z., Chen, C., 2021. Impact of different urban canopy models on air quality simulation in Chengdu, southwestern China. *Atmos. Environ.* 267 <https://doi.org/10.1016/j.atmosenv.2021.118775>.
- Wang, K., Gao, C., Wu, K., Liu, K., Wang, H., Dan, M., Tong, Q., 2023a. ISAT v2.0: an integrated tool for nested-domain configurations and model-ready emission inventories for WRF-AQM. *Geosci. Model Dev.* 16 (7), 1961–1973. <https://doi.org/10.5194/gmd-16-1961-2023>.
- Wang, Y., Jiang, S., Huang, L., Lu, G., Kasemsan, M., Yaluk, E.A., Li, L., 2023b. Differences between VOCs and NO_x transport contributions, their impacts on O₃(3), and implications for O₃(3) pollution mitigation based on CMAQ simulation over the Yangtze River Delta, China. *Sci. Total Environ.* 872, 162118 <https://doi.org/10.1016/j.scitotenv.2023.162118>.
- Wang, N., Du, Y., Chen, D., Meng, H., Chen, X., Zhou, L., Yang, F., 2024. Spatial disparities of ozone pollution in the Sichuan Basin spurred by extreme, hot weather. *Atmos. Chem. Phys.* 24 (5), 3029–3042. <https://doi.org/10.5194/acp-24-3029-2024>.
- Xing, J., Wang, J., Mathur, R., Wang, S., Sarwar, G., Pleim, J., Hao, J., 2017. Impacts of aerosol direct effects on tropospheric ozone through changes in atmospheric dynamics and photolysis rates. *Atmos. Chem. Phys.* 17 (16), 9869–9883. <https://doi.org/10.5194/acp-17-9869-2017>.
- Yang, X., Wu, K., Wang, H., Liu, Y., Gu, S., Lu, Y., Wang, Z., 2020. Summertime ozone pollution in Sichuan Basin, China: meteorological conditions, sources and process analysis. *Atmos. Environ.* 226 <https://doi.org/10.1016/j.atmosenv.2020.117392>.
- Yang, X., Wu, K., Lu, Y., Wang, S., Qiao, Y., Zhang, X., Lei, Y., 2021. Origin of regional springtime ozone episodes in the Sichuan Basin, China: role of synoptic forcing and regional transport. *Environ. Pollut.* 278, 116845 <https://doi.org/10.1016/j.envpol.2021.116845>.
- Yarwood, G., Jung, J., Whitten, G.Z., Heo, G., Mellberg, J., Estes, M., 2010. Updates to the carbon bond mechanism for version 6 (CB6). In: Paper Presented at the 9th Annual CMAS Conference, Chapel Hill, NC.
- Yu, Y., Wang, Z., He, T., Meng, X., Xie, S., Yu, H., 2019. Driving factors of the significant increase in surface ozone in the Yangtze River Delta, China, during 2013–2017. *Atmos. Pollut. Res.* 10 (4), 1357–1364. <https://doi.org/10.1016/j.apr.2019.03.010>.
- Zaveri, R.A., 2003. Ozone production efficiency and NO_x depletion in an urban plume: interpretation of field observations and implications for evaluating O₃-NO_x-VOC sensitivity. *J. Geophys. Res.* 108 (D14) <https://doi.org/10.1029/2002jd003144>.
- Zhang, F., Bei, N., Nielsen-Gammon, J.W., Li, G., Zhang, R., Stuart, A., Aksoy, A., 2007. Impacts of meteorological uncertainties on ozone pollution predictability estimated through meteorological and photochemical ensemble forecasts. *J. Geophys. Res.* 112 (D4) <https://doi.org/10.1029/2006jd007429>.
- Zhang, K., Zhou, L., Fu, Q., Yan, L., Bian, Q., Wang, D., Xiu, G., 2019. Vertical distribution of ozone over Shanghai during late spring: a balloon-borne observation. *Atmos. Environ.* 208, 48–60. <https://doi.org/10.1016/j.atmosenv.2019.03.011>.

- Zhang, S., Lyu, Y., Yang, X., Yuan, L., Wang, Y., Wang, L., Wang, S., 2022. Modeling biogenic volatile organic compounds emissions and subsequent impacts on ozone air quality in the Sichuan Basin, southwestern China. *Front. Ecol. Evol.* 10 <https://doi.org/10.3389/fevo.2022.924944>.
- Zhang, S., Zhang, Z., Li, Y., Du, X., Qu, L., Tang, W., Meng, F., 2023. Formation processes and source contributions of ground-level ozone in urban and suburban Beijing using the WRF-CMAQ modelling system. *J. Environ. Sci. (China)* 127, 753–766. <https://doi.org/10.1016/j.jes.2022.06.016>.
- Zhao, Y., Li, Y., Kumar, A., Ying, Q., Vandenberghe, F., Kleeman, M.J., 2022. Separately resolving NO_x and VOC contributions to ozone formation. *Atmos. Environ.* 285 <https://doi.org/10.1016/j.atmosenv.2022.119224>.
- Zheng, B., Tong, D., Li, M., Liu, F., Hong, C., Geng, G., Zhang, Q., 2018. Trends in China's anthropogenic emissions since 2010 as the consequence of clean air actions. *Atmos. Chem. Phys.* 18 (19), 14095–14111. <https://doi.org/10.5194/acp-18-14095-2018>.